Sciencexpress Report

PAMELA Measurements of Cosmic-Ray Proton and Helium Spectra

O. Adriani,[1,2] G. C. Barbarino,[3,4] G. A. Bazilevskaya,[5] R. Bellotti,[6,7] M. Boezio,[8] E. A. Bogomolov,[9] L. Bonechi,[1,2] M. Bongi,[2] V. Bonvicini,[8] S. Borisov,[10,11,12] S. Bottai,[2] A. Bruno,[6,7] F. Cafagna,[7] D. Campana,[4] R. Carbone,[4,11] P. Carlson,[13] M. Casolino,[10] G. Castellini,[14] L. Consiglio,[4] M. P. De Pascale,[10,11] C. De Santis,[10,11] N. De Simone,[10,11] V. Di Felice,[10] A. M. Galper,[12] W. Gillard,[13] L. Grishantseva,[12] G. Jerse,[8,15] A. V. Karelin,[12] S. V. Koldashov,[12] S. Y. Krutkov,[9] A. N. Kvashnin,[5] A. Leonov,[12] V. Malakhov,[12] V. Malvezzi,[10] L. Marcelli,[10] A. G. Mayorov,[12] W. Menn,[16] V. V. Mikhailov,[12] E. Mocchiutti,[8] A. Monaco,[6,7] N. Mori,[1,2] N. Nikonov,[9,10,11] G. Osteria,[4] F. Palma,[10,11] P. Papini,[2] M. Pearce,[13] P. Picozza,[10,11]* C. Pizzolotto,[8] M. Ricci,[17] S. B. Ricciarini,[2] L. Rossetto,[13] R. Sarkar,[8] M. Simon,[16] R. Sparvoli,[10,11] P. Spillantini,[1,2] Y. I. Stozhkov,[5] A. Vacchi,[8] E. Vannuccini,[2] G. Vasilyev,[9] S. A. Voronov,[12] Y. T. Yurkin,[12] J. Wu,[13]† G. Zampa,[8] N. Zampa,[8] V. G. Zverev[12]

[1]University of Florence, Department of Physics, I-50019 Sesto Fiorentino, Florence, Italy. [2]INFN, Sezione di Florence, I-50019 Sesto Fiorentino, Florence, Italy. [3]University of Naples "Federico II," Department of Physics, I-80126 Naples, Italy. [4]INFN, Sezione di Naples, I-80126 Naples, Italy. [5]Lebedev Physical Institute, RU-119991, Moscow, Russia. [6]University of Bari, Department of Physics, I-70126 Bari, Italy. [7]INFN, Sezione di Bari, I-70126 Bari, Italy. [8]INFN, Sezione di Trieste, I-34149 Trieste, Italy. [9]Ioffe Physical Technical Institute, RU-194021 St. Petersburg, Russia. [10]INFN, Sezione di Rome "Tor Vergata," I-00133 Rome, Italy. [11]University of Rome "Tor Vergata," Department of Physics, I-00133 Rome, Italy. [12]Moscow Engineering and Physics Institute, RU-11540 Moscow, Russia. [13]KTH, Department of Physics, and the Oskar Klein Centre for Cosmoparticle Physics, AlbaNova University Centre, SE-10691 Stockholm, Sweden. [14]IFAC, I-50019 Sesto Fiorentino, Florence, Italy. [15]University of Trieste, Department of Physics, I-34147 Trieste, Italy. [16]Universität Siegen, Department of Physics, D-57068 Siegen, Germany. [17]INFN, Laboratori Nazionali di Frascati, Via Enrico Fermi 40, I-00044 Frascati, Italy.

*To whom correspondence should be addressed. E-mail: picozza@roma2.infn.it
†On leave from School of Mathematics and Physics, China University of Geosciences, CN-430074 Wuhan, China.

Protons and helium nuclei are the most abundant components of the cosmic radiation. Precise measurements of their fluxes are needed to understand the acceleration and subsequent propagation of cosmic rays in the Galaxy. We report precision measurements of the proton and helium spectra in the rigidity range 1 GV-1.2 TV performed by the satellite-borne experiment PAMELA. We find that the spectral shapes of these two species are different and cannot be well described by a single power law. These data challenge the current paradigm of cosmic-ray acceleration in supernova remnants followed by diffusive propagation in the Galaxy. More complex processes of acceleration and propagation of cosmic rays are required to explain the spectral structures observed in our data.

Since the discovery of cosmic rays, various mechanisms have been proposed to explain the acceleration of particles to relativistic energies and their subsequent propagation in the Galaxy. It was pointed out long ago [e.g., (*1*, *2*)] that supernovae fulfill the power requirement to energize galactic cosmic rays. Subsequently, models were put forward explaining the acceleration of cosmic ray particles via diffusive shock acceleration produced by SN (supernova) shock waves propagating in the interstellar medium [see (*3*) for a review].

At the end of the acceleration phase, particles are injected into the interstellar medium where they propagate, diffusing through the turbulent galactic magnetic fields. Nowadays, this propagation is well described by solving numerically (*4*) or analytically (*5*, *6*) the transport equations for particle diffusion in the Galaxy. The galactic magnetic fields mask the arrival direction of charged particles, making the cosmic-ray flux isotropic although there are hints of anisotropy in the 10-100 TeV range (*7*).

Recent PAMELA measurements of the antiparticle component of the cosmic radiation (*8–10*) have prompted a re-evaluation of possible contributions from additional galactic sources, either of astrophysical [e.g., pulsars (*11*)] or exotic [e.g., dark matter (*12*, *13*)] origin. Detailed knowledge of cosmic ray spectra is needed to: (a) identify sources and acceleration/propagation mechanisms of cosmic rays; (b) estimate the production of secondary particles, such as positrons and antiprotons, in order to disentangle the secondary particle component from possible exotic sources; (c) estimate the particle flux in the geomagnetic field and in Earth's atmosphere for in-orbit dose estimations and to derive the atmospheric muon and neutrino flux, respectively.

We present absolute cosmic ray proton and helium spectra in the rigidity interval between 1 GV and 1.2 TV (Fig. 1 and tables S1 and S2), based on data gathered between 2006-2008

with PAMELA, a detector orbiting the Earth in a 350-610 km, 70° inclination orbit as part of the Russian Resurs-DK1 spacecraft (*14*).

Our results are consistent with those of other experiments (Fig. 1), considering the statistical and systematic uncertainties of the various experiments. There are differences at low (< 30 GeV) energies caused by solar modulation effects [PAMELA was operating during a period of minimum solar activity with solar modulation parameter, ϕ, of 450-550 MV in the spherical force field approximation (*15*)]. PAMELA results overlap with ATIC-2 data (*16*) between ~200 and ~1200 GV, but differ both in shape and absolute normalisation at lower energies. The extrapolation to higher energy of the PAMELA fluxes suggest a broad agreement with those published by CREAM (*17*) and JACEE (*18*) but are higher than the RUNJOB (*19*) helium data.

To gain a better understanding of the spectra, we have analysed our results in terms of rigidity instead of kinetic energy per nucleon (Fig. 2 and tables S3 and S4). Two important conclusions can be drawn from the PAMELA data.

Firstly, the proton and helium spectra [$J(R)$] have different spectral shapes. If a single power law, $J\left(R\right) = AR^{-\gamma^R}$, is fit to the data between 30 GV (above the influence of solar modulation) and 1.2 TV, the resulting spectral indices are

$$\gamma^R_{30-1000\,\mathrm{GV,p}} = 2.820 \pm 0.003(stat) \pm 0.005(syst)$$
$$\gamma^R_{30-1000\,\mathrm{GV,He}} = 2.732 \pm 0.005(stat)^{+0.008}_{-0.003}(syst)$$

which establishes that there is a significant difference between the two spectral indices in this rigidity region. These effects are also seen in Fig. 3 (and in table S5), where the proton-to-helium flux ratio is shown as a function of rigidity. Presenting the results as a ratio reduces the possible impact of systematic errors because a number of instrumental effects cancel in the ratio, e.g., the estimation of live time and the error associated with the alignment of the tracker and the track reconstruction algorithm. The proton-to-helium flux ratio shows a continuous and smooth decrease as the rigidity increases. The same ratio cast in terms of kinetic energy per nucleon or total kinetic energy exhibits more irregular behaviour (fig. S1). By applying a power law approximation to the two spectra, the ratio can be used to determine the difference between the two spectral indices with a smaller associated systematic error,

$\Delta_{\gamma^R} = \gamma^R_{\mathrm{p}} - \gamma^R_{\mathrm{He}} = 0.101 \pm 0.0014\left(stat\right) \pm 0.0001\left(sys\right)$

. The ratio is well described by a power law down to rigidities as low as 5 GV (green line in Fig. 3). For rigidities $R >> \phi$, the ratio of the two species is independent of the solar modulation parameter and allows Δ_γ for the interstellar spectrum to be measured in the rigidity range 5-30 GV, where solar modulation effects dominate. Previous measurements (*20–24*) did not have the statistical and systematic precision to demonstrate this decrease in the ratio.

Secondly, as seen in Fig. 4, the PAMELA data show clear deviations from a single power law model. The spectrum of protons gradually softens in the rigidity range 30-230 GV. In the rigidity range 30-80 GV,

$\gamma^R_{30-80\mathrm{GV,p}} = 2.801 \pm 0.007\left(stat\right) \pm 0.002\left(syst\right)$, which is lower than the value fitted between 80-230 GV:

$\gamma^R_{80-230\mathrm{GV,p}} = 2.850 \pm 0.015\left(stat\right) \pm 0.004\left(syst\right)$. In the case of helium,

$\gamma^R_{30-80\mathrm{GV,He}} = 2.71 \pm 0.01\left(stat\right) \pm 0.002\left(syst\right)$, which is lower than

$\gamma^R_{80-230\mathrm{GV,He}} = 2.77 \pm 0.03\left(stat\right) \pm 0.004\left(syst\right)$. We applied Fisher's and Student's *t* tests to the single power law hypothesis in the range 30-230 GV for both protons and helium [see section 5 of the supporting online material (SOM) for details]. This hypothesis is rejected at 95% confidence level (CL). Considering the same rigidity interval in terms of kinetic energy per nucleon the Fisher's and Student's *t* tests reject a single power law hypothesis at 99.7% CL.

At 230-240 GV the proton and helium data exhibit an abrupt spectral hardening. Applying Fisher's test and Student's *t* test to the proton spectrum above 80 GV, the single power law hypothesis is rejected at 99.7% CL if only statistical errors are considered. A similar result is obtained if the fluxes are increased in line with the systematic uncertainties. If the fluxes are instead decreased, the single power law hypothesis is rejected at 95% CL. The hardening of the proton spectrum occurs at 232^{+35}_{-30} GV with change of spectral index from

$\gamma^R_{80-232\mathrm{GV,p}} = 2.85 \pm 0.015\left(stat\right) \pm 0.004\left(syst\right)$ to

$\gamma^R_{>232\mathrm{GV,p}} = 2.67 \pm 0.03 \pm 0.05$. For the helium data, the single power law hypothesis is rejected at 95% CL with spectral hardening setting in at 243^{+27}_{-31} GV and a corresponding change of spectral index of

$\gamma^R_{80-240\mathrm{GV,He}} = 2.766 \pm 0.01 \pm 0.027$ and

$\gamma^R_{>243\mathrm{GV,He}} = 2.477 \pm 0.06 \pm 0.03$. As a consistency check, we repeated this analysis with the three highest energy data points excluded: no changes in the proton and helium results were observed. We obtained similar results when using alternative statistical methods such as the cumulative sum test (see section 5.4 in the SOM).

One of the most striking features of the cosmic rays prior to PAMELA observations was their apparently featureless energy spectra. Until now, single power laws, as predicted by

the shock diffusion acceleration model and diffusive propagation in the Galaxy [see (*25*) for a recent review], could reproduce spectra using similar spectral indices (a fit to the experimental data yields $\gamma \cong 2.7$) for protons and heavier nuclei up to energies of about $\approx 10^{15}$ eV (the so-called "knee" region). Such assumptions are routinely incorporated into common used propagation models, such as GALPROP (*4*), which is widely considered to be the standard model of cosmic-ray acceleration and propagation. Our results challenge this scenario (*26*). As it can be seen in Figs. 2 and 3 the GALPROP calculation does not reproduce PAMELA data across the full rigidity region. Moreover it is difficult, even with recent models of non-linear shock acceleration [e.g., (*27*, *28*)], to produce significant differences in the proton and helium spectra as low as a few tens of GV.

The hardening in the spectra observed by PAMELA around 200 GV could be interpreted as an indication of different populations of cosmic ray sources. As an example of a multi-source model, Fig. 2 shows a comparison with a calculation (blue curves) by Zatsepin and Sokolskaya (*29*), which was put forward to explain ATIC-2 data (*16*) and considered novae stars and explosions in superbubbles as additional cosmic-ray sources. The parameters of the model were fitted to match ATIC-2 data and, consequently, are in disagreement with PAMELA data in absolute fluxes and the ratio. If the parameters of this model are fitted to the PAMELA data the agreement can be greatly improved (red curves of Figs. 2 and 3). CREAM also reported a direct measurement, albeit with a low statistical and systematic significance, of a change of the slope for nuclei ($Z \geq 3$) at 200 GeV/n, i.e. at a higher rigidity($\cong$400 GV) than our observed break in helium spectrum.

An indication that proton and helium have different spectral indices at high energy (~10 TeV) was reported by JACEE (*18*). More recently CREAM (*17*) indirectly inferred [using also AMS (*24*) and BESS (*30*) data] that spectral deformation should occur at about 200 GeV/n for both species. This is similar to our results for protons but higher (400 GV) than our results for helium. Results from ATIC-2 (*16*) implied that protons and helium nuclei have different energy spectra, although the results suffered from unclear systematic uncertainties and there were differences with respect to previously reported ATIC-1 (*31*) data.

References and Notes

1. P. O. Lagage, C. J. Cesarsky, *Astron. Astrophys.* **118**, 223 (1983).
2. V. L. Ginzburg, S. I. Syrovatskii, *The Origin of Cosmic Rays* (Macmillan, New York, 1964).
3. M. A. Malkov, L. O'C Drury, *Rep. Prog. Phys.* **64**, 429 (2001).
4. A. W. Strong, I. V. Moskalenko, *Astrophys. J.* **509**, 212 (1998).
5. F. C. Jones, A. Lukasiak, V. Ptuskin, W. Webber, *Astrophys. J.* **547**, 264 (2001).
6. F. Donato *et al*., *Astrophys. J.* **563**, 172 (2001).
7. M. Amenomori *et al*., *Science* **314**, 439 (2006).
8. O. Adriani *et al*., *Nature* **458**, 607 (2009).
9. O. Adriani *et al*., *Phys. Rev. Lett.* **102**, 051101 (2009).
10. O. Adriani *et al*., *Phys. Rev. Lett.* **105**, 121101 (2010).
11. C. Grimani, *Classical and Quantum Gravity* **26**, 235009 (2009).
12. N. Arkani-Hamed, D. P. Finkbeiner, T. R. Slatyer, N. Weiner, *Phys. Rev. D* **79**, 015014 (2009).
13. G. Kane, R. Lu, S. Watson, *Phys. Lett. B* **681**, 151 (2009).
14. PAMELA comprises a number of high performance detectors, capable of identifying particles through the determination of charge (Z), rigidity ($R = pc/Ze$, p being the momentum of a particle of charge Ze) and velocity ($\beta = v/c$) over a wide energy range. The device is built around a permanent magnet with a 6 plane double-sided silicon micro-strip tracker, providing absolute charge information and track-deflection ($\eta = \pm 1/R$, with the sign depending on the sign of the charge derived from the curvature direction) information. A scintillator system, composed of three double layers of scintillators (S1, S2, S3) provides the trigger, a time-of-flight measurement and an additional estimation of absolute charge. A silicon-tungsten tracking calorimeter, a bottom scintillator (S4) and a neutron detector are used to perform lepton-hadron discrimination. An anticoincidence system is used off-line to reject spurious event triggers generated by particles interacting in the apparatus. Respect to balloon-borne experiments, PAMELA has the advantage of a significantly longer period of uninterrupted observing time. Furthemore, data taking in space is not affected by enviromental systematics such as those due to correction for secondary particles produced in the residual atmosphere that affects balloon-borne experiments. A more detailed description of PAMELA and the analysis methodology can be found in (*32*, *33*) and in the supporting online material.
15. L. J. Gleeson, W. I. Axford, *Astrophys. J.* **154**, 1011 (1968).
16. J. P. Wefel *et al*., *International Cosmic Ray Conference* (2008), vol. 2, pp. 31–34.
17. H. S. Ahn *et al*., *ApJL* **714**, L89 (2010).
18. K. Asakimori *et al*., *Astrophys. J.* **502**, 278 (1998).
19. M. Hareyama, RUNJOB collaboration, *J. Phys. Conf. Ser.* **31**, 159 (2006).
20. W. Menn *et al*., *Astrophys. J.* **533**, 281 (2000).
21. M. Boezio *et al*., *Astrophys. J.* **518**, 457 (1999).
22. M. Boezio *et al*., *Astroparticle Phys.* **19**, 583 (2003).
23. S. Haino *et al*., *Phys. Lett. B* **594**, 35 (2004).
24. J. Alcaraz *et al*., *Phys. Lett. B* **490**, 27 (2000).

25. A. W. Strong, I. V. Moskalenko, V. S. Ptuskin, *Annu. Rev. Nucl. Part. Sci.* **57**, 285 (2007).
26. The changing spectral characteristics of the proton spectrum between 30 and 230 GV may be partly due to heliospheric effects. Although solar modulation effects are considered negligible above 30 GV in the spherical force field approximation (*15*), more detailed models, which use the full Parker equation to describe the propagation of cosmic rays in a two- or three-dimensional heliosphere (*34*, *35*), may be needed to fully understand the impact of this effect.
27. D. Caprioli, P. Blasi, E. Amato, *Astroparticle Physics* arXiv:1007.1925v2 (2010).
28. D. C. Ellison, D. J. Patnaude, P. Slane, P. Blasi, S. Gabici, *Astrophys. J.* **661**, 879 (2007).
29. V. I. Zatsepin, N. V. Sokolskaya, *Astron. Astrophys.* **458**, 1 (2006).
30. T. Sanuki *et al*., *Adv. Space Res.* **27**, 761 (2001).
31. H. S. Ahn *et al*., *Adv. Space Res.* **37**, 1950 (2006).
32. P. Picozza *et al*., *Astroparticle Phys.* **27**, 296 (2007).
33. M. Casolino *et al*., *Adv. Space Res.* **42**, 455 (2008).
34. J. R. Jokipii, E. H. Levy, W. B. Hubbard, *Astrophys. J.* **213**, 861 (1977).
35. M. S. Potgieter, *J. Atmos. Solar-Terrestrial Phys.* **70**, 207 (2008).
36. A. E. Vladimirov *et al*., arXiv:1008.3642v1 (2010).
37. We thank P. Blasi, F. Donato, P. Lipari, and I. Moskalenko for helpful discussions concerning the interpretation of our results and D. Marinucci for helpful discussions on statistical methods. We acknowledge support from the Italian Space Agency (ASI), Deutsches Zentrum für Luft- und Raumfahrt (DLR), The Swedish National Space Board, The Swedish Research Council, The Russian Space Agency (Roscosmos), and The Russian Foundation for Basic Research.

Supporting Online Material

www.sciencemag.org/cgi/content/full/science.1199172/DC1
SOM Text
Figs. S1 to S6
Tables S1 to S7
References

18 October 2010; accepted 9 February 2011
Published online 3 March 2011; 10.1126/science.1199172

Fig. 1. Proton and helium absolute fluxes measured by PAMELA above 1 GeV/n, compared with a few of the previous measurements (*16–24*). All previous measurements but one (*24*) come from balloon-borne experiments. Previous data up to few hundred GeV/n were collected by magnetic spectrometer experiments (*20–24*) while higher energy data come from calorimetric measurements. PAMELA data cover the energy range 1 GeV -1.2 TeV (1-600 GeV/n for He). The fluxes are expressed in terms of kinetic energy per nucleon, converted from the rigidity measured in the tracker and neglecting any contribution from less abundant deuterium (d/p ≅ 1%) and ^{3}He(^{3}He/^{4}He ≅ 10%). Pure proton and ^{4}He samples are therefore assumed. Error bars are statistical, the shaded area represents the estimated systematic uncertainty.

Fig. 2. Proton (top points) and helium (bottom points) data measured by PAMELA in the rigidity range 1 GV-1.2 TV. The shaded area represents the estimated systematic uncertainty. The lines represent the fit with a single power law and the Galprop (*36*) and Zatsepin (*29*) models. Details of the models are presented in tables S1 and S2.

Fig. 3. Ratio of the flux between proton and helium data of PAMELA versus Rigidity. The shaded area represents the estimated systematic uncertainty. Lines show the fit using one single power law (describing the difference of the two spectral indices), the Galprop (*36*) and Zatsepin models with the original values of the paper (*29*) and fitted to the data. Details of the models are presented in tables S1 and S2.

Fig. 4. Proton (left panel) and helium (right panel) spectra in the range 10 GV-1.2 TV. The gray shaded area represents the estimated systematic uncertainty, the pink shaded area represents the contribution due to tracker alignment. The straight (green) lines represent fits with a single power law in the rigidity range 30-240 GV. The red curves represent the fit with a rigidity dependent power law (30-240 GV) and with a single power law above 240 GV.

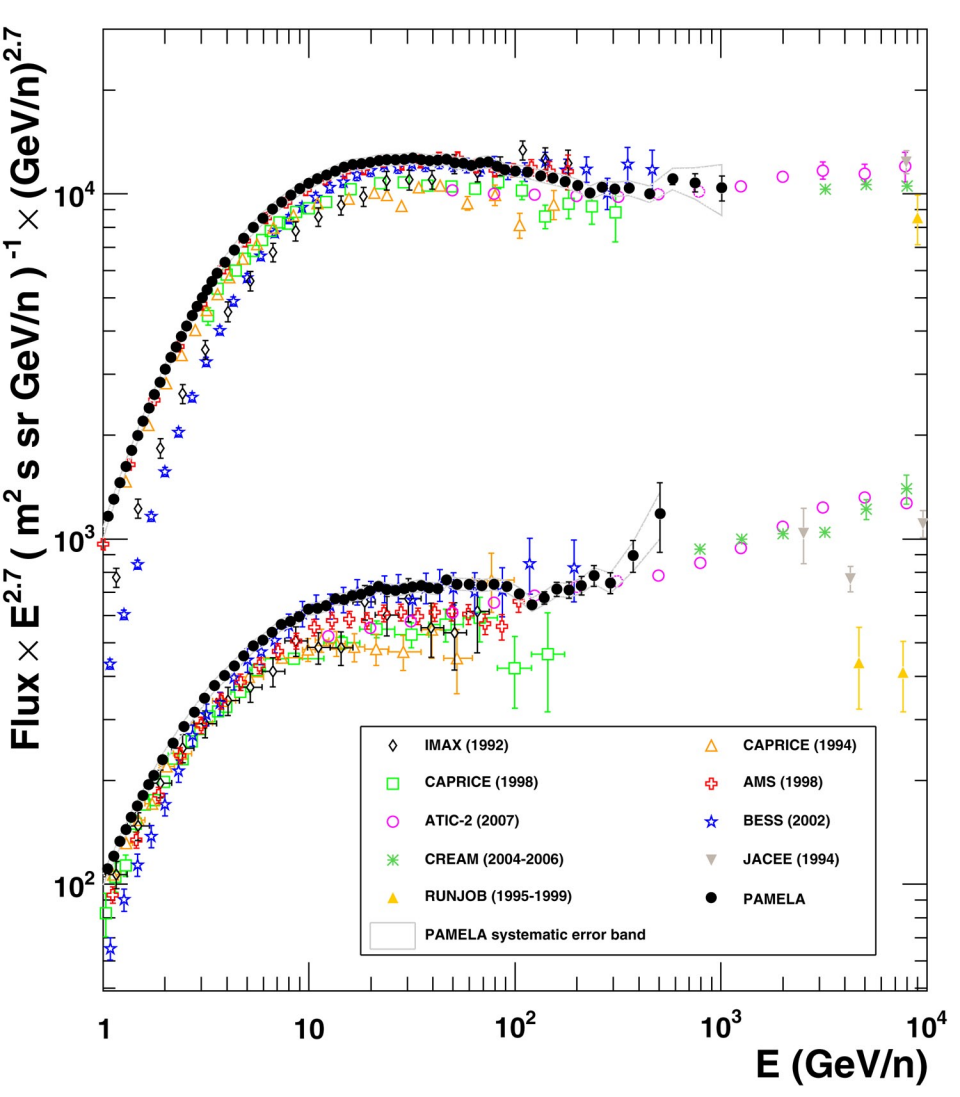
Flux × E^2.7 (m^2 s sr GeV/n)^-1 × (GeV/n)^2.7
10^4
10^3
10^2
1
10
10^2
10^3
10^4
E (GeV/n)
IMAX (1992)
CAPRICE (1994)
CAPRICE (1998)
AMS (1998)
ATIC-2 (2007)
BESS (2002)
CREAM (2004-2006)
JACEE (1994)
RUNJOB (1995-1999)
PAMELA
PAMELA systematic error band

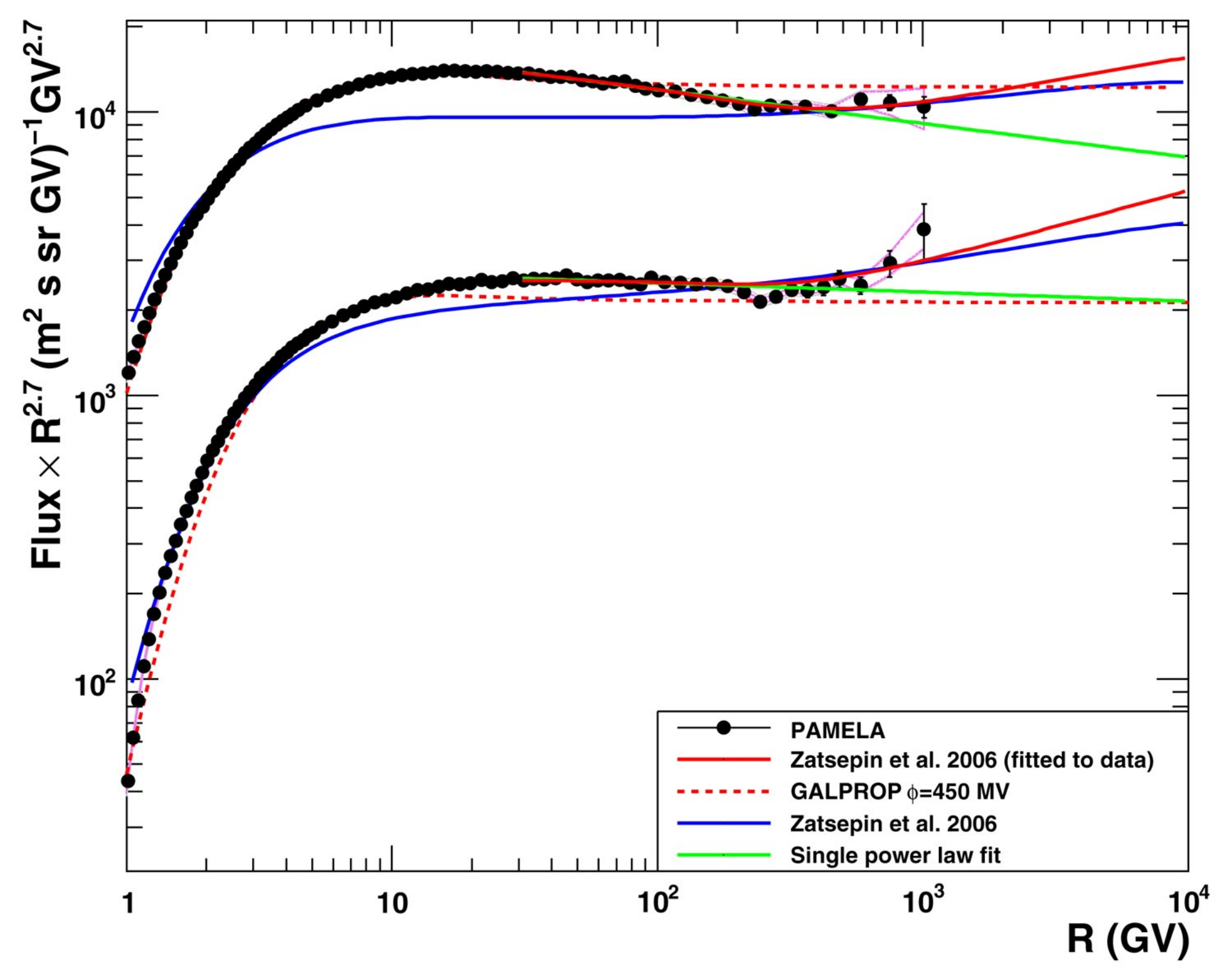
Flux × R^2.7 (m^2 s sr GV)^-1 GV^2.7
10^4
10^3
10^2
1
10
10^2
10^3
10^4
R (GV)
PAMELA
Zatsepin et al. 2006 (fitted to data)
GALPROP ϕ=450 MV
Zatsepin et al. 2006
Single power law fit

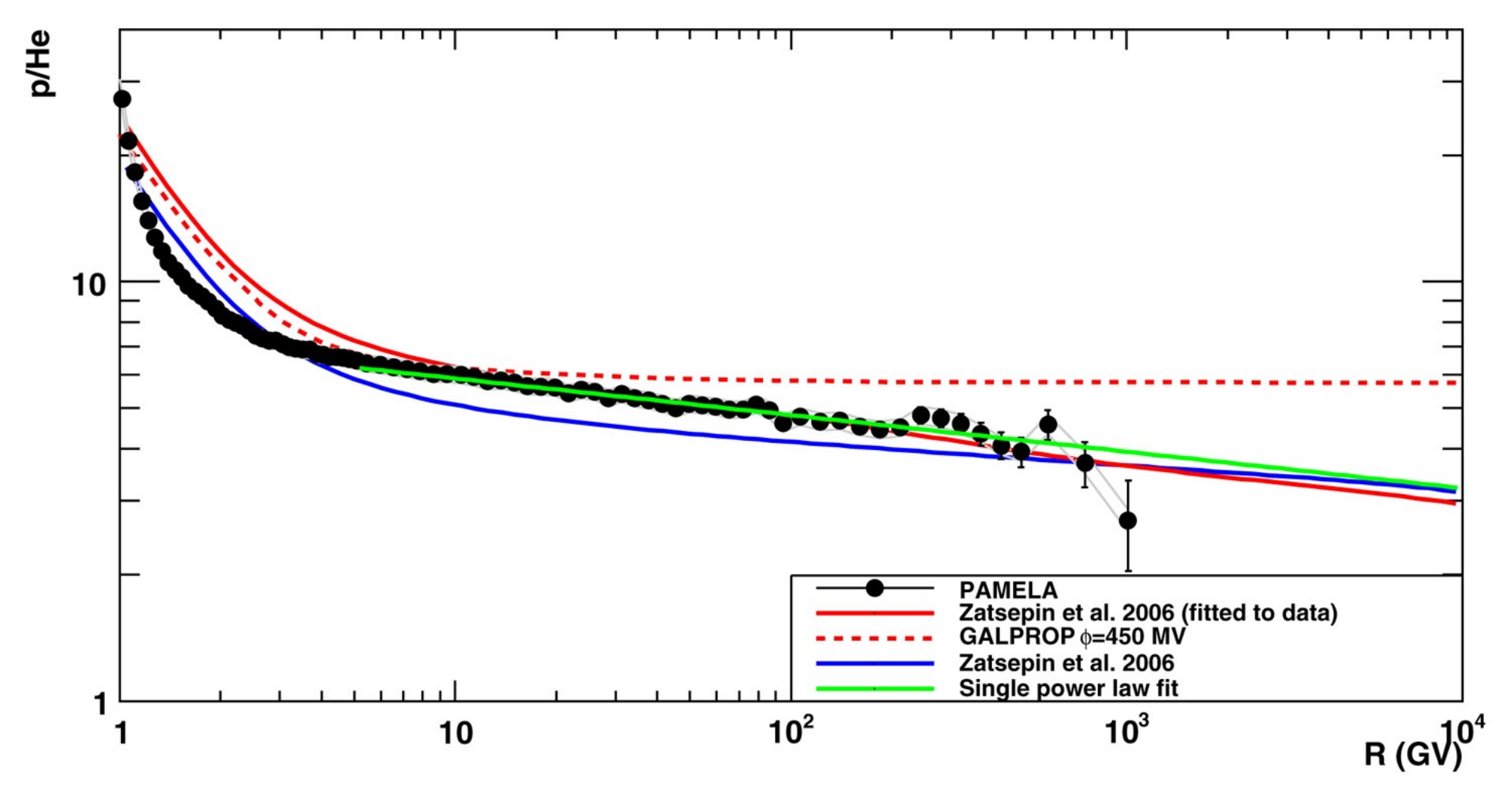
p/He
10
1
1
10
10^2
10^3
10^4
R (GV)
PAMELA
Zatsepin et al. 2006 (fitted to data)
GALPROP ϕ=450 MV
Zatsepin et al. 2006
Single power law fit

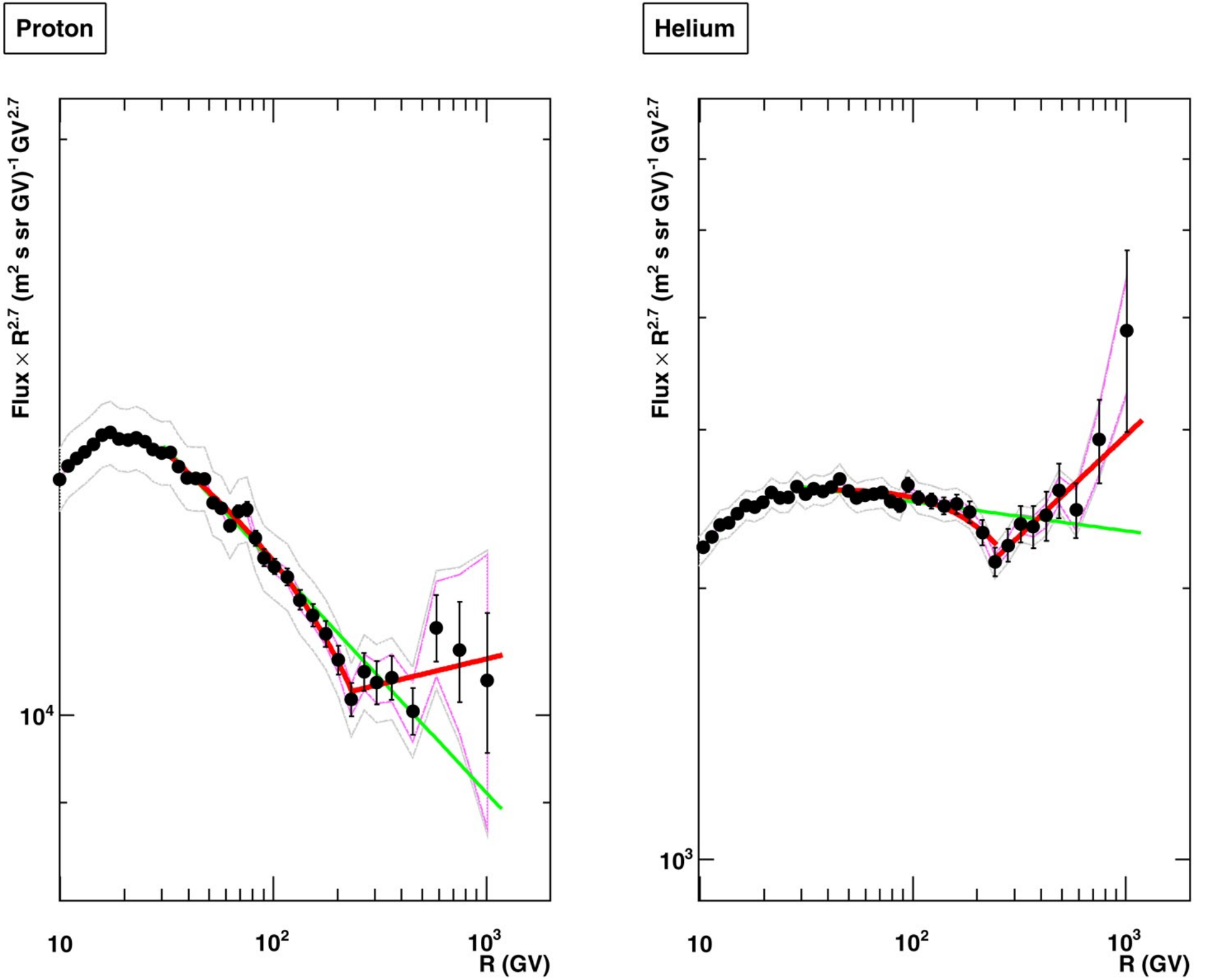
Proton
Helium
Flux × R^2.7 (m^2 s sr GV)^-1 GV^2.7
10^4
10^3
10
10^2
10^3
R (GV)